Automated Design and Characterization of a Scalar Metasurface Antenna Radiating a Linearly-Polarized Broadside Beam

Automated Design and Characterization of a Scalar Metasurface Antenna Radiating a Linearly-Polarized Broadside Beam

Marcello Zucchi*, Andrea Scarabosio†, Francesco Vernì‡, Lucia Teodorani*,
Giorgio Giordanengo†, Giuseppe Vecchi*
*Department of Electronics and Telecommunications, Politecnico di Torino, Turin, Italy, marcello.zucchi@polito.it
†Advanced Computing, Photonics & Electromagnetics (CPE), Fondazione LINKS, Turin, Italy
‡ Huawei Technologies, Milan Research Center, Segrate, Italy

***Abstract*—We present the automated design of a broadside-radiating, linearly-polarized metasurface antenna. The design is carried out with a numerical optimization procedure based on the equivalent surface current only. A non-linear conjugate gradient algorithm is applied to minimize an objective function that includes both realizability and far field requirements. A suitable configuration of circular unit cells, chosen from a database of precomputed shapes, is then used to implement the antenna. The proposed antenna has a diameter $\approx 12\lambda$, working at a frequency of 23 GHz. The obtained design has been validated with commercial software simulations, then prototyped and tested.**

I. Introduction

As the demand for compact, efficient, and multifunctional antennas continues to grow in the era of wireless communication and sensing, metasurface antennas have emerged as a promising solution. These antennas harness the principles of metasurfaces, engineered two-dimensional structures composed of subwavelength scatterers or resonators, to control and manipulate electromagnetic waves with unprecedented precision and versatility [1].

Due to the multi-scale nature of these antennas, with small scattering elements arranged over large areas, the design is characterized by a large number of degrees of freedom, making a direct design not feasible in most practical cases. The design is addressed by modeling the metasurface as a layer of Impedance Boundary Condition (IBC), enabling the use of efficient numerical techniques.

For the IBC design, various approaches have been put forth; some rely on analytical approximations [2], while others are based on numerical methods [3]. For the case of scalar metasurfaces, the current-based design method described by the authors in [4] has the benefit of not requiring any prior knowledge of the impedance profile (a reduced order parameterization is not required), making it particularly suitable for situations in which the profile is not known analytically, such as shaped beams.

The design of a circular metasurface radiating a linearly-polarized, broadside beam is used to test the capabilities of the aforementioned approach. Following the automated design, the impedance has been implemented with circular patches and the final antenna layout prototyped and tested. The proposed design was first presented in [5], although only preliminary, simulated results were provided. Here, we deal with the full design cycle: starting from the details of the automated design, we arrive at the manufactured prototype and compare the related measurements with simulations.

II. Synthesis of Metasurface Antennas

A. IBC Synthesis

A locally variable scalar Impedance Boundary Condition (IBC) is used to macroscopically model the behavior of a metasurface.

$$\boldsymbol{E}_{\mathrm{t}} = Z_{\mathrm{s}}\, \boldsymbol{J}_{\mathrm{s}} \tag{1}$$

Impedance values are constrained to be reactive in the case of lossless scatterers, i.e., $Z_{\mathrm{s}} = \mathrm{j}X_{\mathrm{s}}$. The problem is formulated as an integral equation (EFIE-IBC),

$$\boldsymbol{E}_{\mathrm{inc}} + \mathcal{L}\boldsymbol{J} = Z\boldsymbol{J}, \tag{2}$$

where $\boldsymbol{E}_{\mathrm{inc}}$ is the incident (source) field, while $\mathcal{L}$ is the Electric Field Integral Operator. The current is expanded as a linear combination of RWG basis function and the discretization of the problem follows the usual Method of Moments procedure with Galerkin testing.

The IBC synthesis follows the method presented in [4]. It is based on the optimization of the surface current through the minimization of a single objective function that embeds all *design requirements* (pattern masks, impedance range) and *physical constraints* (passivity, losslessness):

$$\mathsf{I}^{\star} = \underset{\mathsf{I}\in\mathbb{C}^{N}}{\arg\min}\, (f_{\mathrm{rlz}}(\mathsf{I}) + f_{\mathrm{rad}}(\mathsf{I})) \tag{3}$$

where

$$f_{\mathrm{rlz}} = \sum_{i=1}^{N_{\mathrm{c}}} \rho_i^{\mathrm{act}} + \sum_{i=1}^{N_{\mathrm{c}}} \rho_i^{\mathrm{rct}} + \sum_{i=1}^{N_{\mathrm{c}}} \rho_i^{\mathrm{scal}} \tag{4}$$

$$f_{\mathrm{rad}} = \rho^{\mathrm{ref}} + \sum_{j\in\mathrm{ML}} (\rho_j^{\mathrm{co}} + \rho_j^{\mathrm{cx}}) + \sum_{j\in\mathrm{SL}} \rho_j^{\mathrm{tot}} \tag{5}$$

Here, ρ_i^{act}, ρ_i^{rct}, ρ_i^{scal} are the functionals for passivity, impedance range and scalarity constraints respectively; ρ^{ref} is

the functional for the gain maximization, while ρ_j^{co}, ρ_j^{cx}, ρ_j^{tot} are functionals that encode the co-, cross-polarization and total field (sidelobes) constraints.

All these functionals are dependent on the current coefficients I and are formulated as 4^{th}-order piece-wise polynomials of the form

$$\rho_i(\mathsf{I}) = \mathrm{r}^2\left(\mathsf{I}^{\mathsf{H}}\mathbf{A}_i\mathsf{I} + \mathsf{I}^{\mathsf{H}}\mathsf{b}_i + c_i\right) \tag{6}$$

where $\mathbf{A}_i \in \mathbb{C}^{N\times N}$ is hermitian, $\mathsf{b} \in \mathbb{C}^N$, and $c_i \in \mathbb{C}$. The continuous function $\mathrm{r}(x) = \max(x, 0)$ is used to treat inequalities (masks) constraints.

The function is minimized with a *non-linear conjugate gradient algorithm*, with a modified line-search procedure in order to exploit the polynomial structure. This formulation also allows the use of fast numerical routines for electromagnetic analysis in the computation of the gradients. In this way, the algorithm is applicable to large structures with an approximately log-linear scaling of the numerical complexity with respect to the antenna size [4].

Finally, from the optimized current and the corresponding electric field, the impedance is obtained with a local minimization of the squared error in the EFIE-IBC equation over each individual cell domain $\mathcal{S}_i$,

$$Z_i = \frac{\langle \boldsymbol{E}^\star_{\tan}, (\boldsymbol{J}^\star)^* \rangle_{\mathcal{S}_i}}{\|\boldsymbol{J}^\star\|^2_{\mathcal{S}_i}}, \tag{7}$$

where $\boldsymbol{J}^\star = \sum_n I_n^\star \boldsymbol{f}_n$ and $\boldsymbol{E}^\star_{\tan} = \boldsymbol{E}_{\mathrm{inc}} + \mathcal{L}\boldsymbol{J}^\star$. Any residual real part of the impedance is set to zero to ensure losslessness. Areas that display a very low current magnitude are considered open circuit conditions, which are treated by removing the corresponding triangles and basis functions from the discretization.

B. Unit-cell database

A pre-computed database of unit-cell shapes is used in the construction of the metasurface derived from the optimized impedance profile. By running simulations for each possible shape, within a periodic approximation, it is possible to extract the equivalent impedance values [6].

For the scalar impedance case, the considered unit-cells are *circular patches* with varying radius. The unit cell has a side length of $L = \lambda/6 = 2.2$ mm and the radius varies from $0.5L$ to $0.9L$ for a total number of 1000 different shapes. This corresponds to a reactance (imaginary part of the impedance) range from $-1500\,\Omega$ to $-100\,\Omega$

III. Results

The circular metasurface has been designed at a frequency of 23 GHz and has a diameter $D = 158$ mm $\approx 12\ \lambda$. The grounded dielectric substrate has a thickness $h = 0.508$ mm, a diameter of 180 mm, and $\varepsilon_{\mathrm{r}} = 3.34$. The antenna is fed by a central vertical pin exciting a surface wave. The cylindrical pin has a diameter of 0.9 mm and an height of 3.159 mm above the ground plane. The latter has been optimized to maximize the input matching.

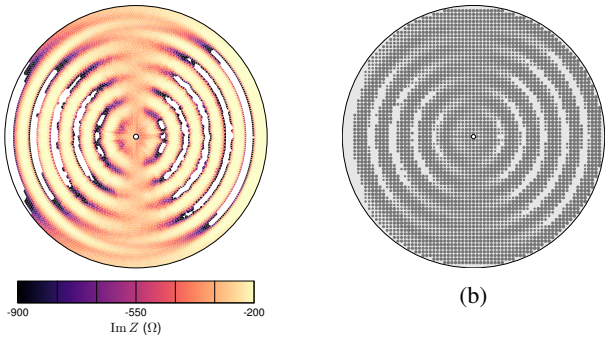

(a) (b)

Fig. 1: Circular MTS antenna with linear pol. broadside radiation: (a) Optimized continuous impedance profile, (b) implementation with circular unit-cells.

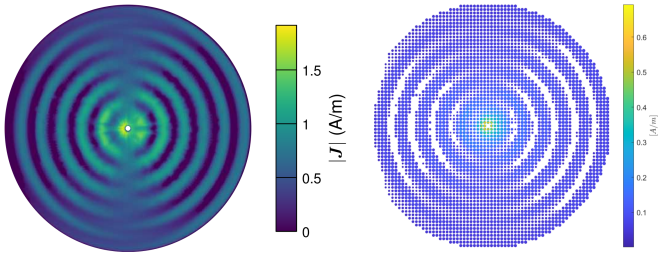

(a) (b)

Fig. 2: Circular MTS antenna with linear pol. broadside radiation: (a) Optimized surface current profile, (b) simulated surface current with unit-cell implementation.

The numerical modelling includes 32 472 RWG basis functions for the surface discretization, and the incident field is computed as the analytical TM_0 surface-wave mode.

The desired broadside beam has a $10°$ HPBW, linear polarization along the x-axis, with cross-polarization and sidelobes levels below -25 dB. The surface reactance is constrained within $-1000\,\Omega$ and $-200\,\Omega$.

Fig. 1a and Fig. 1b show the optimized IBC profile and its associated implementation. The impedance profile mimics previously published analytical profiles for linear polarization [7], [8], and is symmetric, as predicted by the symmetry of the radiation constraints. These results were obtained without any a priori information on the impedance profile, in a fully automated way.

The final design has been simulated with the time domain solver in CST. Fig. 2 shows the comparison between the optimized current profile and the surface current on the individual patches obtained from full-wave simulation. Afterwards, the antenna has been manufactured on a MEGTRON 7 substrate (Fig. 3), and tested in an anechoic chamber.

The resulting directivity pattern is shown in Fig. 4 for the two principal cuts, together with the pattern constraints. The co-polarization component complies with the requirements, with a maximum directivity of 22.5 dB (15% aperture ef-

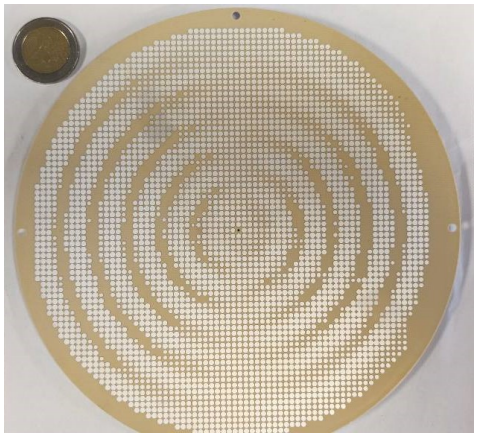

Fig. 3: Prototype of the designed circular MTS antenna.

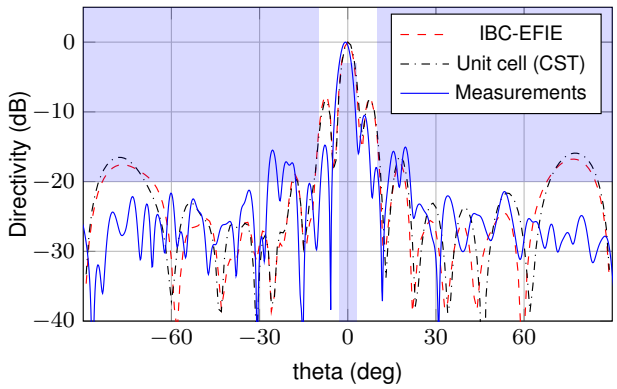

(a) $\varphi = 0°$

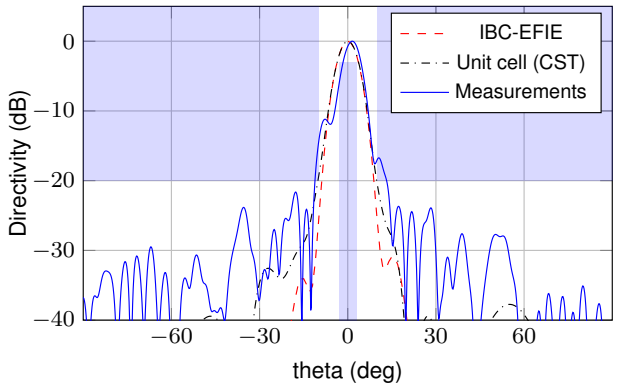

(b) $\varphi = 90°$

Fig. 4: Co-polar normalized directivity for the circular MTS antenna: (a) $\varphi = 0°$, (b) $\varphi = 90°$. "IBC-EFIE" refers to the pattern obtained with a continuous impedance profile.

ficiency). As widely documented in the literature, radiation performance can be significantly improved by using a tensorial impedance profile.

IV. Conclusions

The design of a linearly-polarized, broadside beam radiating MTS antenna has been presented. It has been carried out with a fully automated process, by first designing the IBC surface through a current-based optimization, and then implementing it with circular patches. The resulting antenna layout has been first verified through commercial software simulations, then prototyped and tested. Measurements showed a satisfactory agreement with respect to the designed performance, demonstrating the effectiveness of the proposed approach.

Acknowledgement

This work was supported by the Italian Ministry of Research project PRIN 2020EY2LJT "METEOR".

References

[1] M. Faenzi, G. Minatti, D. González-Ovejero, F. Caminita, E. Martini, C. D. Giovampaola, and S. Maci, "Metasurface Antennas: New Models, Applications and Realizations," *Sci Rep*, vol. 9, no. 1, pp. 1–14, Jul. 2019.

[2] G. Minatti, F. Caminita, M. Casaletti, and S. Maci, "Spiral Leaky-Wave Antennas Based on Modulated Surface Impedance," *IEEE Trans. Antennas Propag.*, vol. 59, no. 12, pp. 4436–4444, Dec. 2011.

[3] M. Bodehou, C. Craeye, and I. Huynen, "Electric Field Integral Equation-Based Synthesis of Elliptical-Domain Metasurface Antennas," *IEEE Trans. Antennas Propag.*, vol. 67, no. 2, pp. 1270–1274, Feb. 2019.

[4] M. Zucchi, F. Vernì, M. Righero, and G. Vecchi, "Current Based Automated Design of Realizable Metasurface Antennas With Arbitrary Pattern Constraints," *IEEE Trans. Antennas Propag.*, vol. 71, no. 6, pp. 4888–4902, Jun. 2023.

[5] M. Zucchi, A. Scarabosio, M. Righero, G. Giordanengo, F. Vernì, and G. Vecchi, "Automated Design of a Broadside-Radiating Linearly Polarized Isotropic Metasurface Antenna," in *2023 IEEE Int. Symp. Antennas Propag. USNC-URSI Radio Sci. Meet. USNC-URSI*, Jul. 2023, pp. 1767–1768.

[6] A. M. Patel and A. Grbic, "Modeling and Analysis of Printed-Circuit Tensor Impedance Surfaces," *IEEE Trans. Antennas Propag.*, vol. 61, no. 1, pp. 211–220, Jan. 2013.

[7] A. Arroyo, R. Contreres, A. Piche, H. Roussel, and M. Casaletti, "Linear Polarization from Scalar Modulated Metasurfaces," in *2022 16th Eur. Conf. Antennas Propag. EuCAP*, Mar. 2022, pp. 1–4.

[8] D. González-Ovejero, N. Chahat, R. Sauleau, G. Chattopadhyay, S. Maci, and M. Ettorre, "Additive Manufactured Metal-Only Modulated Metasurface Antennas," *IEEE Trans. Antennas Propag.*, vol. 66, no. 11, pp. 6106–6114, Nov. 2018.